

Combining Fault Tolerance Techniques and COTS SoC Accelerators for Payload Processing in Space

Vasileios Leon*, Elissaios Alexios Papatheofanous[†], George Lentaris*,
Charalampos Bezaitis[†], Nikolaos Mastorakis*, Georgios Bampilis*, Dionysios Reisis[†], Dimitrios Soudris*

*School of Electrical and Computer Engineering, National Technical University of Athens, 15780 Athens, Greece

[†]Department of Physics, National and Kapodistrian University of Athens, 15772 Athens, Greece

Abstract—The ever-increasing demand for computational power and I/O throughput in space applications is transforming the landscape of on-board computing. A variety of Commercial-Off-The-Shelf (COTS) accelerators emerges as an attractive solution for payload processing to outperform the traditional radiation-hardened devices. Towards increasing the reliability of such COTS accelerators, the current paper explores and evaluates fault-tolerance techniques for the Zynq FPGA and the Myriad VPU, which are two device families being integrated in industrial space avionics architectures/boards, such as Ubotica's CogniSat, Xiphos' Q7S, and Cobham Gaisler's GR-VPX-XCKU060. On the FPGA side, we combine techniques such as memory scrubbing, partial reconfiguration, triple modular redundancy, and watchdogs. On the VPU side, we detect and correct errors in the instruction and data memories, as well as we apply redundancy at processor level (SHAVE cores). When considering FPGA with VPU co-processing, we also develop a fault-tolerant interface between the two devices based on the CIF/LCD protocols and our custom CRC error-detecting code.

Index Terms—Fault Tolerance, Reliability, Space Avionics, Mixed-Criticality, COTS Components, Zynq FPGA, Myriad VPU

I. INTRODUCTION

The “NewSpace” era relies on novel technological approaches in space applications. The advances in small form factor satellites, such as SmallSats and CubeSats, broaden the scope of the Earth Observation (EO) missions and attract new areas of research for payload processing in space. In particular, challenges such as the increased data generated by satellite instruments and computational demands of modern Digital Signal Processing (DSP) and Artificial Intelligence (AI) algorithms, constrained by the power budget and dependability requirements of each space mission, drives the industry to revisit the computing architectures for space avionics.

Classical space-qualified general-purpose processors, such as the radiation-hardened Power-PC and LEON CPUs [1], fail to follow the aforementioned trend. As a result, the industry turns to mixed-criticality architectures. These heterogeneous architectures combine rad-hard components and Commercial-Off-The-Shelf (COTS) accelerators for payload processing and especially image processing applications that are not mission-critical [2]. Specialized COTS System-on-Chip (SoC), such as Vision Processing Units (VPUs) and SoC Field-Programmable Gate Arrays (FPGAs), offer attractive trade-offs between Size,

Weight, Power and Cost (SWaP-C), processing performance and development flexibility [3], [4]. However, despite their benefits, these COTS devices are not radiation hardened by design, and thus, they are susceptible to ionizing radiation increasing the risk of failures. To tackle this risk, Fault-Tolerance (FT) architectures and fault-mitigation techniques need to be designed. Commonly used techniques include rad-hard components supervising the COTS ones, Error Correction Coding (ECC) and Error Detection and Correction (EDAC) in memories, and Triple Modular Redundant (TMR) processing.

Recent works in the literature showcase combinations of fault-mitigation techniques at different levels of computing architectures for space applications [5]–[7]. In [5], platform-level FT is developed, where 3 distinct Myriad2 VPUs operate in TMR mode. In this architecture, the Cobham Gaisler's GR-VPX-XCKU060 board [8] integrates Xilinx's Kintex Ultra-Scale XCKU060 FPGA for voting and the radiation-tolerant GR716 microcontroller acting as supervisor. In [6], the authors utilize a COTS Xilinx Zynq MPSoC for payload processing, which is partitioned between isolated secure/non-secure areas based on the criticality of the application executed on them, while a rad-hard PolarFire FPGA supervises. The work in [7] introduces hardening techniques in a system with two redundant Zynq UltraScale+ MPSoCs for accelerating neural-network-based hyperspectral image segmentation. The supervisor is a Vorago Cortex-M0 microcontroller, which also implements EDAC/ECC in all internal memories.

The current work explores, combines, and evaluates fault-mitigation techniques for a COTS-based mixed-criticality architecture targeting the acceleration of payload functions. Our HW architecture consists of a SoC FPGA and Myriad2 VPU pair with diverse implementations, which vary from interconnecting low-end readily-available COTS boards to developing high-end custom-made PCBs (depending on mission requirements and budget availability). Our SW layer, which is the focus of this paper, consists of a combination of techniques trading off reliability and performance overheads (also depending on mission specifications). On the FPGA side, we implement mitigation techniques for the FPGA configuration memory and process, as well as modular redundancy for the payload processing acceleration. On the VPU side, we apply error correction to both instruction and working memory as

well as modular redundancy of processing cores. Furthermore, we develop FT communication for the payload data transfers between FPGA and VPU via the CIF and LCD interfaces. Finally, we design a supervising scheme, where each one device acts as an individual watchdog of the second device, while monitoring its status over UART. We test an engineering model of the proposed system by utilizing simple COTS boards, i.e., a Xilinx Zynq-7000 SoC FPGA and the Intel Myriad2 VPU, where all of our mitigation techniques are evaluated. For the evaluation of our techniques, we adopt a fault emulation/injection setup. The results show that our robust FT architecture on Zynq maintains correct functionality for the 72% of the time even during an extreme test involving 10K injections per 40s. On the Myriad2 side, we ensure error-free application results with an overhead of ~ 50 ms.

II. COTS-BASED FPGA & VPU ARCHITECTURE

As a proof-of-concept, we assume here the instantiation of the FPGA & VPU architecture depicted in Fig. 1, which enables us to study our SW layer of mitigation techniques. Flight models can rely on more sophisticated HW configurations and PCBs. More precisely, depending on mission specifics, we identify three potential HW implementation levels in an ascending order of development cost and tolerance:

- Xilinx Zybo FPGA + Ubotica CogniSat or EoT VPU
- Xiphos Q7S (with daughter card) + GR-HPCB-FMC-M2
- custom PCB with redundant FPGA and/or VPU units

The first level involves relatively ubiquitous boards and targets low-cost CubeSats. For more advanced CubeSats, the second level involves commercial space-oriented boards, e.g., Xiphos Q7S [9] with extra FMC adaptor card enabling the Cobham Gaisler GR-HPCB-FMC-M2 daughterboard [5] to connect and maximize the FPGA-VPU bandwidth. The third level involves customized PCB designs targeting even microsatellites, e.g., similarly to our previous work [10] (but with Zynq).

The current paper assumes the first implementation level (Zybo plus CogniSat [11] or EoT [12]) with the FPGA handling the payload sensors/instruments (Fig. 1), e.g., via SpaceWire as in our previous work [4]. The FPGA performs mostly data transcoding and DSP acceleration, while it also encodes and forwards instrument data to the VPU via CIF. The VPU mostly accelerates DSP/AI workloads. The VPU results are received by the FPGA via UART. The boards' interconnection relies on available pins, e.g., on CogniSat's hardwired CIF pins and Zybo's GPIOs for CIF. The UART interface can also facilitate our watchdog policies. Boards can be externally reset via dedicated pins. We note that CIF/LCD FPGA-VPU interconnections were also developed in our previous work [10].

III. MITIGATION TECHNIQUES ON ZYNQ FPGA

In the Zynq FPGA (left side of Fig. 2), the ARM-based Processing System (PS) is used for monitoring the FT techniques, while the Programmable Logic (PL) is used for implementing the accelerators and all the required FT components.

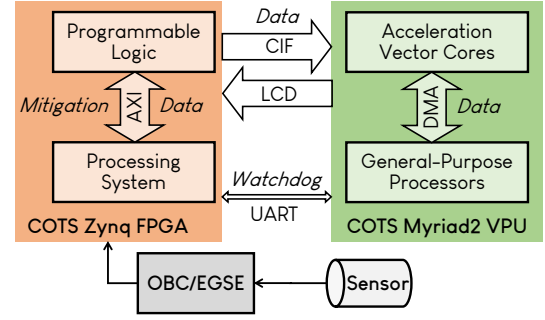


Fig. 1. High-level COTS co-processing architecture with Zynq and Myriad2.

A. CMS: Configuration Memory Scrubbing

Our design for scrubbing Zynq's configuration memory is based on Xilinx's SEM IP. This IP utilizes the internal readback CRC hardware to perform error detection using the built-in ECC and CRC codes, as shown in Fig. 3a. The Frame ECC interface is used to access the configuration memory checksum when a memory frame is read. The Zynq PS communicates with SEM via the AXI UART interface, receiving information about the status of SEM, as well as transmitting commands to SEM. The Data Fetch interface is a mechanism allowing SEM to fetch data from an external memory, i.e., the chip's QSPI flash memory in our case, and perform memory scrubbing via the ICAP interface. In our design, we configure SEM to "replace" mode, which applies data-reload-based correction of the configuration memory frames.

B. DPR: Dynamic Partial Reconfiguration

In case a small part of the design needs to be modified due to errors, we employ dynamic partial reconfiguration. As shown in Fig. 3b, partial bitstreams are delivered to the ICAP via the AXI HWICAP IP core using the ARM processor and the AXI lite protocol. In particular, a software running on ARM is responsible for reading bitstream data from the the QSPI flash memory and feeding them to ICAP via AXI HWICAP.

C. TMR: Triple Modular Redundancy

Our third FT technique is the classic TMR, which, however, is tailored to the Zynq architecture as shown in Fig. 3c. Besides only triplicating the main accelerator implemented on the FPGA, we also applying voting on the input data that are transferred to PL from PS via AXI. Correspondingly, we apply voting on the PS side to ensure that the correct output data are transferred to ARM.

D. Hybrid Fault-Tolerant Architectures

At first, we apply both DPR and CMS (for memory correction) along with TMR (for application-level protection), while we also combine all three techniques. Finally, to increase the robustness of the system, we develop an architecture where all the proposed FT techniques are applied in cooperation with a watchdog policy (WD) running on an external microcontroller (prototyped with Arduino). In particular, if any of the TMR components are permanently faulty, we apply partial reconfiguration. At the same time, the SEM controller

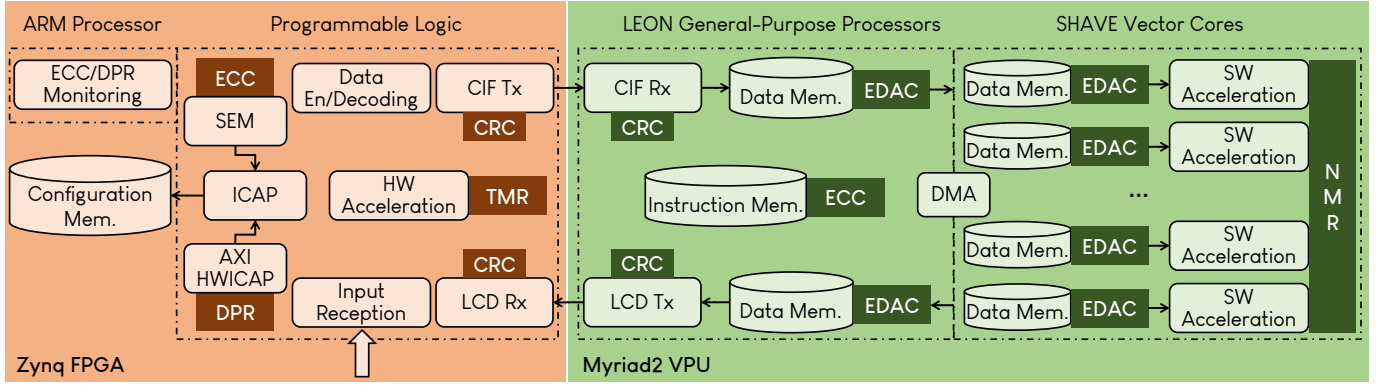


Fig. 2. Main components and dataflow of FT co-processing architecture based on Zynq and Myriad2.

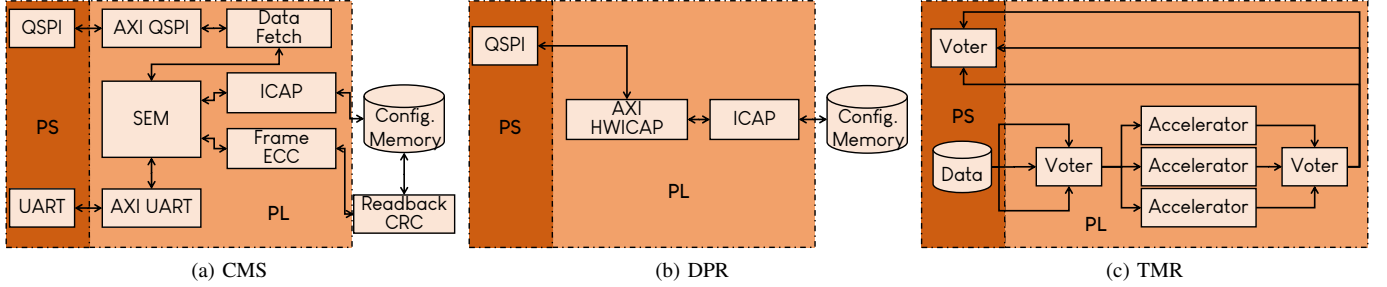


Fig. 3. FT techniques on Zynq: (a) Configuration Memory Scrubbing, (b) Dynamic Partial Reconfiguration, and (c) Triple Modular Redundancy.

performs CMS and provides a message to the watchdog timer via UART. In case the timer expires, we reset the entire SoC FPGA by using the configuration data stored in the QSPI flash memory. The combination of all the FT techniques imposes some limitations. Both CMS and DPR use the ICAP peripheral for reconfiguring the FPGA. Therefore, ICAP is available only to SEM or HWICAP to apply CMS or DPR, respectively. Moreover, in the WD-based architecture, we configure SEM to “enhanced repair” mode (ECC and CRC algorithm-based correction), as QSPI is needed for booting the device.

IV. MITIGATION TECHNIQUES ON MYRIAD2 VPU

In the Myriad2 VPU (right side of Fig. 2), the general-purpose LEON core is the orchestrator of the entire dataflow, while it also implements the FT techniques. The input data are received and stored in the DDR global memory, and then, they are transferred via DMA to the scratchpad 2MB-size CMX memory, where they are processed by the 12 SHAVE cores (VLIW & SIMD processors). We note that the developer manually divides the workload to tasks and assigns them to SHAVES. Below, we present the FT techniques for Myriad2.

A. IMR: Instruction Memory Recovery

Our first fault-tolerant technique targets to correct errors in the instruction memory of SHAVES, which are the main acceleration cores. The developer can specify the memory space of the SHAVES’ code either in DDR or CMX, thus, LEON knows the instruction memory space of each SHAVE core. In this technique, illustrated in Fig. 4a, LEON initially calculates the CRC values of all the instruction memory space. Therefore, at runtime, it can check if the memory contents

have changed through the repeated calculation of the CRC. Considering that the SHAVE code is not modified at runtime, any change in these memory locations indicates fault. In such case, LEON detects the SHAVES corresponding to corrupted memory locations and sends their input data to the remaining functional SHAVES to calculate the correct results. Upon finishing the the re-execution, LEON recovers the impaired SHAVES using a golden copy of the instruction memory (stored in DDR or external memory).

B. DMR: Data Memory Recovery

A similar CRC-based approach, illustrated in Fig. 4b, is used to confront errors in the data. Besides the CRC calculations for the data received via CIF (presented in Section V), we detect errors in the data after their on-chip DMA transmission in the CMX scratchpad memory, where they are directly accessed and processed by SHAVES. LEON appends a CRC value to each input data tile, and the corresponding SHAVE calculates the CRC value before starting the processing. In case of errors in the data of some SHAVES, LEON restores the input data (e.g., by using a golden copy such as in the case of the instruction memory), and then, re-schedules the execution on the functional SHAVES.

C. NMR: N Modular Redundancy

In this technique, instead of parallelizing the workload to the 12 SHAVE cores, we create groups of N SHAVES and assign them the same input data for processing. LEON receives their outputs and executes a voting system to retain the correct result. This process is illustrated in Fig. 4c. For $N=3$, we have 4 groups of SHAVES, i.e., in practice the workload

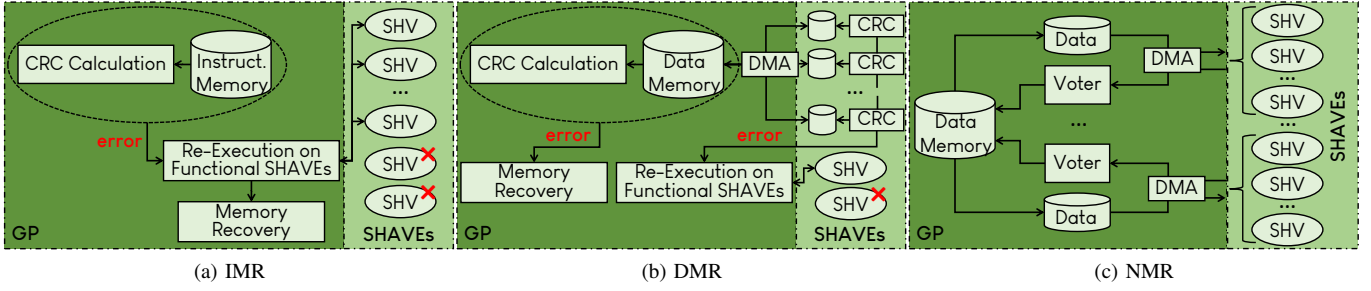


Fig. 4. FT techniques on Myriad2: (a) Instruction Memory Recovery, (b) Data Memory Recovery, and (c) N Modular Redundancy.

is parallelized to 4 cores. For $N=5$, we have 4 groups of SHAVEs, while we do not use 2 cores at all.

V. FAULT-TOLERANT FPGA-VPU COMMUNICATION

The payload data communication between the FPGA and VPU is performed over the CIF and LCD interfaces in the form of image frames and is designed to be fault-tolerant. In particular, payload data frames exchanged between both sides are protected by a 16-bit CRC field. The CRC values are appended to the end of each frame by means of a frame footer. The footer has the form of an entire CIF or LCD frame row with the first pixels containing the 16-bit CRC, while the rest pixels are zero-padded. The CRC algorithm used for both CIF and LCD is CRC-16-CCITT, where the polynomial is $0x1021$ ($x^{16} + x^{12} + x^5 + 1$) with an initial value of $0x0$.

On the FPGA side, the module that is responsible for formulating and appending the CRC on CIF frames transmitted to the VPU is shown in Fig. 5a. While a CIF frame transmission is active, the CIF CRC module reads one pixel value at each clock cycle from a pixel buffer and forwards it to the CIF transmitter. The CIF transmitter supports frames with bit-depth of 8, 16 and 24. For this, the CIF CRC contains three instances of a CRC16 calculator (based on linear-feedback shift register), which operate in parallel and calculate on-the-fly the CRC values of frames with 8, 16 and 24-bit depth. The CRC16 calculators are controlled by the counter-based Frame Footer FSM. When the active portion of the frame has been forwarded, the CRC16 calculation is complete. Then, the Frame Footer FSM selects the output of the CRC16 calculators based on the corresponding bit-depth and forwards the additional footer row that contains the CRC16 value in the first pixel(s). When the entire CIF frame is received on the VPU side, the VPU calculates the corresponding CRC16 value and compares it with the received one.

The transmission of LCD frames from the VPU to the FPGA follows the same principles as that of CIF frames. When an LCD frame of payload data has been formulated in the VPU, the VPU calculates the CRC16 value, includes it to the footer of the frame and starts the frame transmission over LCD. The module that handles the CRC calculation and comparison on the FPGA side is shown in Fig. 5b. The LCD receiver feeds the LCD CRC module with one pixel value at each clock cycle. Three distinct CRC16 modules operate in parallel on different bit-widths of the incoming pixel in order to support

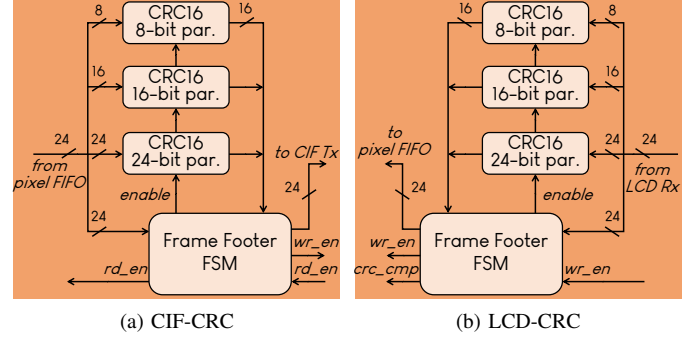


Fig. 5. CRC modules implemented on the FPGA for FT communication.

all the three different frame bit-depths. When the active portion of the LCD frame has been received, the CRC16 value is calculated and the Frame Footer FSM handles the reception of the additional footer row. It extracts the received CRC value from the correct position of the footer and performs the comparison with the calculated one. The comparison result is reported to the corresponding status registers of the FPGA.

VI. EXPERIMENTAL EVALUATION

A. Test Setup

For the experimental evaluation, we use the Zybo board (Zynq-7010) along with the associated software tools, i.e., Xilinx's Vivado and SDK, and the Myriad2 VPU along with Intel's MDK design suite. As benchmarks, we use an FIR filter for the FPGA and two image processing software kernels (averaging binning and floating-point convolution) for the VPU. The FIR filter is developed with VHDL on the PL of Zynq, and applies pipelined filtering for streaming input, while its coefficients are stored in a ROM mapped onto LUTs. The VPU benchmarks are parallelized to the 12 SHAVE cores, i.e., the input image is divided into stripes that are assigned to SHAVEs for parallel processing. The general-purpose LEON processor performs all the necessary high-level tasks, e.g., SHAVE initialization, stripe partition, and DMA transfers.

Zynq FPGA: To emulate errors in the FPGA, we inject faults in Zynq's configuration memory using the SEM-based ACME tool [13]. This tool translates the essential memory bits, which are provided in the so-called EBD ASCII file, into injection addresses for SEM. ACME also provides subsets of essential

bits that correspond to the components of the design, allowing to perform injection campaigns for specific design parts. For injecting faults, the Zynq PS sends commands to SEM via AXI-UART, specifying the bit locations in the memory frame addresses. The successful fault injection is indicated by status signals, while the SEM controller transitions from the injection state to idle to wait for the next injection command.

Myriad2 VPU: Intel does not provide any fault-injection framework such as SEM, thus, we develop our own methods for inserting faults in the data and instructions memories. Regarding data, we consider three approaches that are based on random-number routines: (i) LEON corrupts the input data (stored in DDR) before transferring them to CMX to be processed by SHAVEs, (ii) SHAVEs corrupt their own input data upon receiving them, (iii) LEON corrupts the shared variables between it and SHAVEs. Similarly, we assign LEON to corrupt the instructions (code) of SHAVEs (stored in DDR).

B. FPGA Results

We employ a test involving 10K fault injections inserted in the configuration memory every 4ms. Our injection campaign targets the utilized FPGA area (FT components + application).

The results of Table I show the portion of time that the FPGA is non-functional (down) and has erroneous/correct functionality. As shown, the standalone application of each FT technique improves the downtime from 92% to 73–80%, with CMS exhibiting the correct functionality for more time (22% vs. 1–8%). The advantage of CMS is that it detects the errors when they generated (it checks the memory and does not wait for a new output, i.e., like TMR). Furthermore, TMR provides near-zero correct functionality, as our injection campaign targets the TMR modules and after the $\sim 2K$ injections the system is down. Nevertheless, when combining TMR with either CMS or DPR, the functionality of the FPGA is improved. On the one hand, this is due to the errors being distributed across a larger design, but also because TMR notifies in time DPR to act and increases the time for CMS to correct the errors. The combination of all three FT techniques increases the reliability of the system even more, as the FPGA operates correctly for half of the test duration. Finally, the benefit of additionally using WD is that, besides quickly detecting errors by both TMR and CMS, it captures the case that the CMS design has a permanent fault. As a result, it significantly increases the robustness of the system, providing correct execution for 72% of time. Based on the same test, Fig. 6 demonstrates the reliability of the FT architectures over time. We assume exponentially-distributed random faults at rate λ and that the system reliability is defined as $R(t) = e^{-\lambda \cdot t}$ [14]. The pattern remains the same, as the most reliable architectures are the combined one. However, DPR provides less reliability, as it lacks an error detection mechanism contrary to the other techniques.

Table II shows that all the FT architectures exhibit small resource utilization ($<4K$ LUTs, $<5K$ FFs, <6 RAMBs). Therefore, there is room for the implementation of other components required in the co-processing architecture, e.g.,

TABLE I
FPGA TEST: 10K FAULT INJECTIONS IN UTILIZED AREA (ONE PER 4MS)

FT Architecture	Downtime / No Functionality	Erroneous Functionality	Correct Functionality
No FT (app only)	92%	8%	0%
TMR	80%	19%	1%
DPR	79%	13%	8%
CMS	73%	5%	22%
DPR + TMR	36%	41%	23%
CMS + TMR	31%	24%	45%
CMS + DPR + TMR	27%	22%	51%
CMS + DPR + TMR + WD	20%	8%	72%

¹ % refers to portion of time of the total test duration.

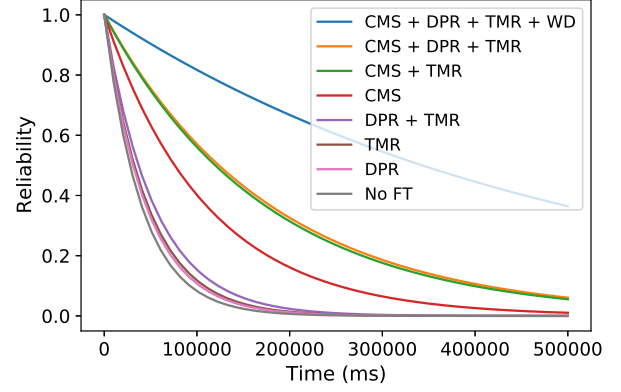


Fig. 6. FPGA reliability (failure probability) w.r.t. to the FT techniques (legend sorted based on declining reliability).

TABLE II
RESOURCE UTILIZATION OF FT TECHNIQUES ON ZYNQ-7010

FT Architecture	LUTs	FFs	RAMBs
No FT (app only)	609 (4%)	1461 (4%)	1 (2%)
TMR	1316 (8%)	2327 (7%)	4 (7%)
DPR	1315 (8%)	2501 (7%)	0 (0%)
CMS	2021 (12%)	2761 (8%)	2 (3%)
DPR + TMR	2022 (12%)	3367 (10%)	4 (7%)
CMS + TMR	2727 (16%)	3801 (11%)	6 (10%)
CMS + DPR + TMR	3433 (20%)	4841 (14%)	6 (10%)
CMS + DPR + TMR + WD	3756 (21%)	5072 (14%)	6 (10%)

more DSP functions, data transcoders and data compressors. In more detail, the SEM IP of the CMS technique imposes the largest resource overhead. The resource increment in the WD-based FT architecture is due to: (i) the UART communication between the watchdog (microcontroller) and the FPGA, and (ii) the “enhanced repair” mode of SEM (instead of “replace”). Finally, according to our measurements, SEM corrects a memory frame of 404 bytes in 18ms (“enhanced repair”), while the throughput of DPR via HWICAP is 67 MB/s.

C. VPU Results

For the Myriad2 VPU, we examine the error rate, i.e., the number of erroneous pixels per total pixels, as well as the timing overheads for providing FT processing. Our tests involve the random injection of errors in the instruction and data memories of 3, 6, 9, or 12 SHAVE cores.

TABLE III
ERROR RATE OF FT PROCESSING ON MYRIAD2 VPU

Benchmark		Impaired SHAVE Cores			
		3	6	9	12
No FT (app only)	Conv2D	13–25%	24–50%	31–74%	44–99%
	Binn2D	9–25%	12–48%	16–74%	24–97%
IMR DMR NMR	Conv2D	0–13%	0–48%	0–74%	0–99%
	Binn2D	0–11%	0–48%	0–69%	0–97%

¹ Impaired SHAVE refers to faults in its data or instruction memory.

² The errors in FT processing remain in the NMR technique.

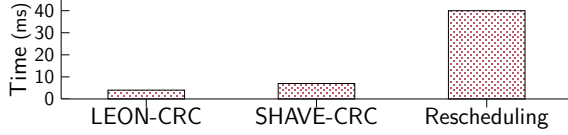


Fig. 7. Overhead of main tasks for FT processing on Myriad2 VPU.

Table III reports the range of the error rate for all our tests without and with the FT techniques. The convolution kernel provides less error resilience than averaging binning, however, as expected, their error rate reaches almost 100% when corrupting the memories of all 12 SHAVES. The application of either IMR or DMR, i.e., the CRC-based FT techniques that reschedule the workload of impaired SHAVES, eliminates the errors. Regarding the standalone application of NMR i.e., without rescheduling, most of the errors remain, especially when corrupting ≥ 6 SHAVES (because 2 or more cores of the same voting group are impaired).

In terms of timing overhead, NMR is equivalent to applying 4-core ($N=3$) and 2-core ($N=5$) rather than 12-core parallelization. Namely, there is an almost linear decrease in the application latency (when also considering the voting overhead). For IMR and DMR, Fig. 7 shows the execution times of their main tasks. The CRC calculations are small (< 10 ms), while the rescheduling (data re-arrangement and assignment to non-impaired SHAVES) requires ~ 40 ms on average. Nevertheless, both techniques achieve correct application execution.

D. Communication Results

Regarding the FPGA–VPU communication, the VHDL design for the CIF transmitter and LCD receiver, including the CRC modules, can achieve an operating frequency of 100MHz on the PL of Zynq-7010. The resource utilization for both the receiver and transmitter as well as the additional CRC modules is shown in Table IV. We observe that the fault-tolerance CRC functionality of the communication adds small resource overhead, which is similar to that of the FT techniques.

Given that the VHDL can support the frequency of 100MHz, the actual operating frequency and achievable throughput for reliable communication depends on the I/O capabilities of different hardware setups. For example, in commercial hardware, a Xiphos Q7S board with a custom mezzanine daughter card connected to an Eyes Of Things (EoT) Myriad2 board over jumper wires can support reliable transmission over CIF for frames of 1024×1024 , 16-bit pixels at 50MHz. The same connectivity principles can be applied to the space-oriented COTS Myriad2 CogniSat platform. The

TABLE IV
RESOURCES FOR FT FPGA–VPU COMMUNICATION ON ZYNQ-7010

Component	LUTs	FFs	DSPs	RAMBs
CIF Tx + LCD Rx	2977 (17%)	1232 (4%)	2 (3%)	10 (17%)
CIF-CRC + LCD-CRC	347 (2%)	305 (1%)	2 (3%)	0 (0%)

FPGA–VPU communication can scale up to both CIF & LCD operating reliably up to 150MHz for 2048×2048 , 24-bit frames in custom hardware setups for space applications, where the FPGA and Myriad2 are connected over a custom FMC Mezzanine connector as in [5] and [10].

VII. CONCLUSION

We developed, proposed, and combined various FT techniques for the Zynq FPGA and the Myriad2 VPU, i.e., two COTS chips already being considered for space missions. We prototyped an FPGA & VPU co-processing architecture based on available COTS boards, we evaluated techniques for error correction in memories, accelerator redundancy, watchdog timers, and data transmission based on CRC. We showed that FPGA reliability gets significantly increased via our robust hybrid FT architecture, which utilizes ~ 4 K LUTs to provide correct functionality for 72% of the time during very demanding tests. Regarding Myriad2, we achieve error-free execution with an overhead of up to ~ 50 ms. Future work will include engineering models with space-heritage components.

REFERENCES

- [1] V. Leon *et al.*, “Development and Testing on the European Space-Grade BRAVE FPGAs: Evaluation of NG-Large Using High-Performance DSP Benchmarks,” *IEEE Access*, vol. 9, pp. 131 877–131 892, 2021.
- [2] G. Furano *et al.*, “Towards the Use of Artificial Intelligence on the Edge in Space Systems: Challenges and Opportunities,” *IEEE Aerospace and Electronic Systems Magazine*, vol. 35, no. 12, pp. 44–56, 2020.
- [3] G. Lentar *et al.*, “High-Performance Vision-Based Navigation on SoC FPGA for Spacecraft Proximity Operations,” *IEEE Trans. on Circuits and Systems for Video Technology*, vol. 30, no. 4, pp. 1188–1202, 2020.
- [4] V. Leon *et al.*, “Improving Performance-Power-Programmability in Space Avionics with Edge Devices: VBN on Myriad2 SoC,” *ACM Trans. on Embedded Computing Systems*, vol. 20, no. 3, pp. 1–23, 2021.
- [5] J. E. Navarro *et al.*, “High-Performance Compute Board – A Fault-Tolerant Module for On-Board Vision Processing,” in *Europ. Workshop on On-Board Data Processing (OBDP)*, 2021, pp. 1–7.
- [6] R. C. Amorim *et al.*, “Dependable MPSoC Framework for Mixed Criticality Applications,” in *Europ. Workshop on On-Board Data Processing (OBDP)*, 2021.
- [7] P. Kuligowski *et al.*, “System-Level Hardening Techniques Used in the COTS-based Data Processing Unit,” in *Europ. Workshop on On-Board Data Processing (OBDP)*, 2021.
- [8] Cobham Gaisler, *GR-VPX-XCKU060*, (accessed May 2022). [Online]. Available: <https://www.gaisler.com/index.php/products/boards/gr-vpx-xcku060>
- [9] Xiphos, *Q7*, (accessed May 2022). [Online]. Available: <https://xiphos.com/products/q7-processor/>
- [10] V. Leon *et al.*, “FPGA & VPU Co-Processing in Space Applications: Development and Testing with DSP/AI Benchmarks,” in *IEEE Intl. Conference on Electronics, Circuits, & Systems (ICECS)*, 2021, pp. 1–5.
- [11] Ubotica, *CogniSat*, (accessed May 2022). [Online]. Available: <https://ubotica.com/product/specifications/>
- [12] O. Deniz *et al.*, “Eyes of Things,” *MDPI Sensors*, vol. 17, no. 5, pp. 1–29, 2017.
- [13] L. A. Aranda *et al.*, “ACME: A Tool to Improve Configuration Memory Fault Injection in SRAM-Based FPGAs,” *IEEE Access*, vol. 7, pp. 128 153–128 161, 2019.
- [14] F. Afsharnia, “Failure Rate Analysis,” in *Failure Analysis and Prevention*. IntechOpen, 2017, ch. 7.